Journal of Controlled Release 146 (2010) 219–227

Contents lists available at ScienceDirect

Journal of Controlled Release

journal homepage: www.elsevier.com/locate/jconrel

Tumor-homing multifunctional nanoparticles for cancer theragnosis: Simultaneous diagnosis, drug delivery, and therapeutic monitoring

Kwangmeyung Kim [a,1], Jong Ho Kim [b,1], Hyungkyu Park [a], Yoo-Shin Kim [c], Kyeongsoon Park [a,b], Heayun Nam [a,d], Seulki Lee [a], Jae Hyung Park [d], Rang-Woon Park [c], In-San Kim [c], Kuiwon Choi [a], Sang Yoon Kim [e], Kinam Park [b,*], Ick Chan Kwon [a,*]

[a] Biomedical Research Center, Korea Institute of Science and Technology, 39-1 Haweolgog-Dong, Sungbook-Gu, Seoul 136-791, South Korea
[b] Departments of Biomedical Engineering and Pharmaceutics, Purdue University, West Lafayette, IN 47907, United States
[c] Advanced Medical Technology Cluster for Diagnosis and Prediction, Kyungpook National University, Daegu 700-422, South Korea
[d] Department of Life and Nanopharmaceutical Sciences, Kyung Hee University, Dongdaemun-gu, Seoul 130-701, South Korea
[e] Department of Otolaryngology, Asan Medical Center, College of Medicine, University of Ulsan, 388-1 Pungnap-dong, Songpa-gu, Seoul 138-736, South Korea

ARTICLE INFO

Article history:
Received 3 December 2009
Accepted 4 April 2010
Available online 24 April 2010

Keywords:
Theragnosis
Chitosan nanoparticle
Paclitaxel
Tumor homing
Drug delivery
Non-invasive imaging

ABSTRACT

Theragnostic multifunctional nanoparticles hold great promise in simultaneous diagnosis of disease, targeted drug delivery with minimal toxicity, and monitoring of treatment. One of the current challenges in cancer treatment is enhancing the tumor-specific targeting of both imaging probes and anticancer agents. Herein, we report tumor-homing chitosan-based nanoparticles (CNPs) that simultaneously execute cancer diagnosis and therapy (cancer theragnosis). These CNPs are unique for their three distinctive characteristics, such as stability in serum, deformability, and rapid uptake by tumor cells. These properties are critical in increasing their tumor targeting specificity and reducing their nonspecific uptake by normal tissues. To develop these CNPs into novel theragnostic nanoparticles, we labeled them with Cy5.5, a near-infrared fluorescent (NIRF) dye, for imaging and also loaded them with paclitaxel (PTX-CNPs), an anticancer drug, for cancer treatment. Cy5.5 labeled PTX-CNPs exhibited significantly increased tumor-homing ability with low nonspecific uptake by other tissues in SCC7 tumor-bearing mice. Theragnostic nanoparticles, Cy5.5 labeled PTX-CNPs, are highly useful for simultaneous diagnosis of early-stage cancer and drug delivery.

1. Introduction

Recently, nanotechnology and molecular imaging have been combined to generate multifunctional nanoparticles that simultaneously facilitate cancer theragnosis [1]. Theragnostic nanoparticles show great promise in the emerging field of personalized medicine, because they allow detection as well as monitoring of an individual patient's cancer at an early-stage, and delivering anticancer agents over an extended period for enhanced therapeutic efficacy. Moreover, real-time, non-invasive monitoring of the theragnostic nanoparticles enables clinicians to rapidly decide whether the regimen is effective in an individual patient or not [2]. For these reasons, cancer theragnosis with multifunctional nanoparticles presents a promising new strategy in cancer treatment. Successful clinical applications of cancer theragnosis require discovery of highly efficient tumor-homing nanoparticles which can diagnose and deliver targeted therapy.

Cancer researchers have been actively exploring various tumor targeting nanoparticles made of lipid-based micelles, natural/synthetic polymeric particles, and inorganic particles for cancer theragnosis [3–5]. However, the results of tumor targeting have not been as good as one would expect from the targeted delivery, and this may be due to the factors that are not well understood in tumor targeting by nanodelivery systems. Nanoparticles with the size in the range of 200 nm are known to accumulate at the solid tumor site by the so-called enhanced permeation and retention (EPR) effect, resulting in efficient accumulation in solid tumor tissues [6]. Unfortunately, if we examine the reported literature data carefully, *in vivo* studies have shown that the tumor specificity of the nanoparticles was only slightly better than the controls. Nanoparticles introduced into the circulating blood are quickly removed by the immune system from the body [7,8]. Indeed, a number of nanoparticles with different characteristics (e.g., different surface chemistry, size, surface charge, and molecular weight) were proven unsatisfactory in *in vivo* tests with regard to stability, biodistribution, and tumor targeting specificity [9,10]. Furthermore, the final *in vivo* destination of nanoparticles has been

* Corresponding authors. Kwon is to be contacted at Biomedical Research Center, Korea Institute of Science and Technology, 39-1 Haweolgog-Dong, Sungbook-Gu, Seoul 136-791, South Korea. Park, Departments of Biomedical Engineering and Pharmaceutics, Purdue University, West Lafayette, IN 47907, United States.
E-mail addresses: kpark@purdue.edu (K. Park), ikwon@kist.re.kr (I.C. Kwon).
[1] These authors contributed equally to this paper.

0168-3659/$ – see front matter © 2010 Elsevier B.V. All rights reserved.
doi:10.1016/j.jconrel.2010.04.004

largely unknown, because it is difficult to acquire direct and non-invasive images on the nanoparticles in animal studies.

Herein, we introduce a new concept for creating theragnostic nanoparticles that was based on polymeric nanoparticle technology and molecular imaging. We designed tumor-homing chitosan-based nanoparticles (CNPs) containing a near-infrared fluorescent (NIRF) dye and an anticancer drug (Fig. 1A) [11–13]. Unlike other nanoparticles commonly used in drug delivery, these CNPs are more efficiently localized at tumor tissues by the EPR effect. These tumor-homing profiles of the CNPs *in vivo* were monitored and compared with control carrier systems, such as water-soluble polymer and polymeric beads, in tumor-bearing mice by non-invasive optical fluorescence image. Furthermore, the theragnostic potential of the drug-loaded CNPs was evaluated by their tumor specificity, targeted delivery of the drug and *in vivo* monitoring of therapeutic responses, simultaneously.

2. Materials and methods

2.1. Synthesis of theragnostic chitosan-based nanoparticles

Synthetic details of Cy5.5-labeled and PTX-encapsulated chitosan-based nanoparticles (PTX-CNPs) are described in Supplementary information. Briefly, first, water-soluble glycol chitosan (GC, Mw = 250 kDa) were chemically modified with hydrophobic 5β-cholanic acid in the presence of N-hydroxysuccinimide (NHS) and 1-ethyl-3-(3-dimethylaminopropyl)-carbodiimide hydrochloride (EDAC), as previously reported [14–17]. The freshly synthesized glycol chitosan-5β-cholanic acid conjugates had 150 ± 4.5 molecules of hydrophobic 5β-cholanic acids per one glycol chitosan (glycol chitosan-5β-cholanic acid$_{150}$, Mw = 301 kDa). Second, the glycol chitosan-5β-cholanic acid conjugates were labeled with the NIRF dye, hydroxysuccinimide ester of Cy5.5. On average, each molecule of glycol chitosan-5β-cholanic acid contained 4.8 ± 0.7 molecules of Cy5.5 (Cy5.5$_{4.8}$-glycol chitosan-5β-cholanic aicd$_{150}$, Mw = 306 kDa). Finally, 10 wt.% of water insoluble paclitaxel (PTX) was encapsulated into the Cy5.5 labeled CNPs by a simple dialysis method (see Supplementary information). The produced Cy5.5 labeled and PTX-encapsulated CNPs (PTX-CNPs) with a higher drug loading efficiency of 92% were well dispersed in distilled water and PBS under sonication. As control nanoparticles, polystyrene bead (PS) containing amine moieties (Polybead® Amino Micospheres 0.2 μm, Polysciences, Inc. Warrington, PA) were also labeled with monoreactive hydroxysuccinimide ester of Cy5.5 and the Cy5.5 labeled PS particles were used as rigid and non-deformable particles *in vitro* and *in vivo* experiments.

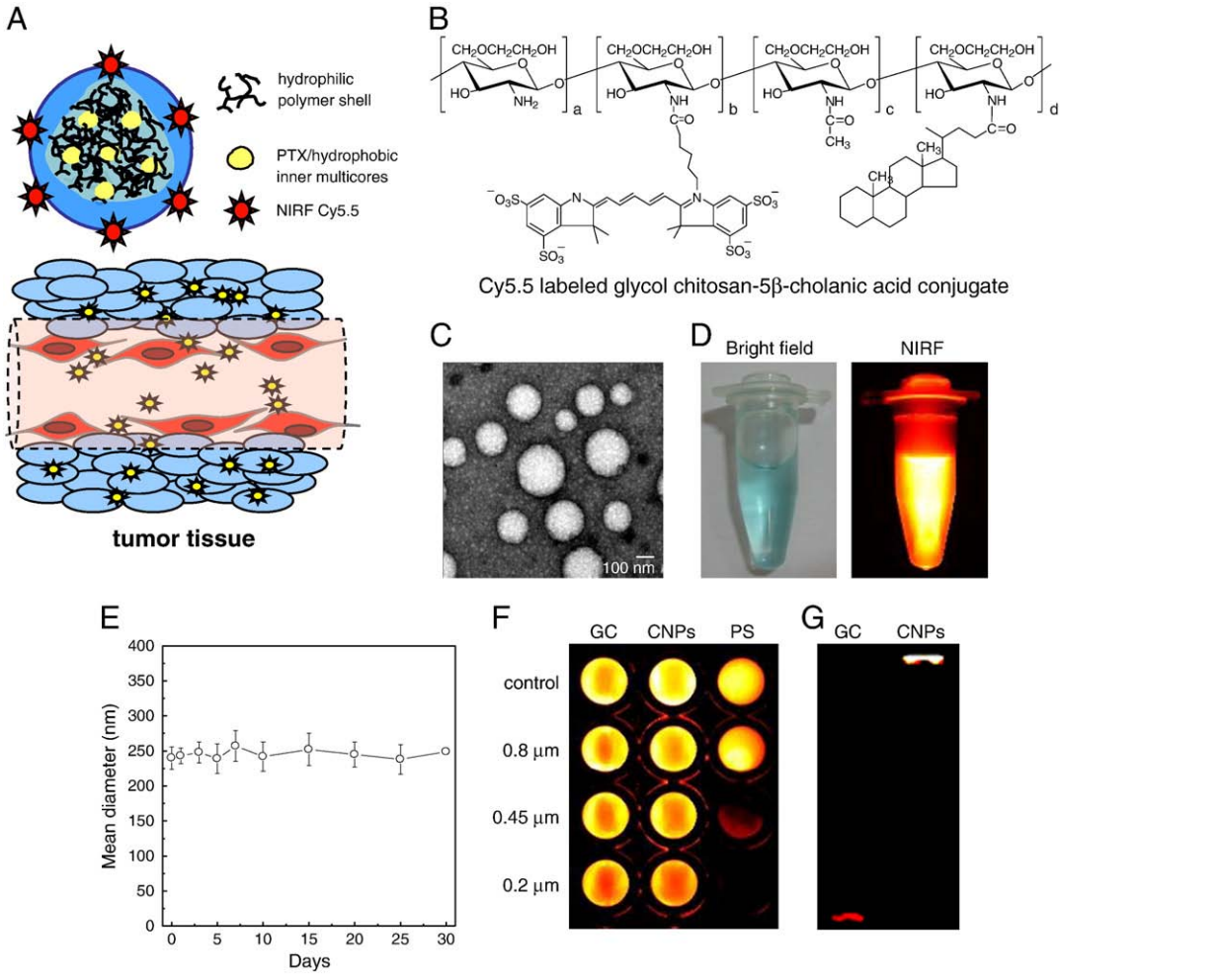

Fig. 1. (A) Conceptual description of a theragnostic nanoscale particle designed for cancer imaging and treatment. The theragnostic chitosan-based nanoparticles (CNPs) can preferentially accumulate at the tumor tissue by the enhanced permeation and retention (EPR) effect due to their unique properties, such as stability in blood, deformability, and fast cellular uptake. (B) Chemical structure of the glycol chitosan conjugates labeled with Cy5.5, a near-infrared fluorescent (NIRF) dye, and modified with hydrophobic 5β-cholanic acid. (C) A TEM image of Cy5.5-labeled CNPs (1 mg/ml) in distilled water. (D) Bright field and NIRF images of the Cy5.5-labeled CNPs in PBS. The NIRF image was obtained using a Cy5.5 filter set (ex = 674 nm, em = 695 nm). (E) Time-dependant size distribution of Cy5.5-labeled CNPs in PBS at 37 °C was confirmed using dynamic light scattering. (F) Filtration of water-soluble glycol chitosan (GC), CNPs, and polystyrene (PS) beads through filters of different pore sizes (0.8 μm, 0.45 μm, and 0.2 μm). The amount of each particle passed through the filters was quantified through NIRF intensity of the filtrate. (G) *In vitro* stability of the Cy5.5-labeled CNPs was determined using an SDS-PAGE test. Cy5.5-labeled GC polymers and CNPs were incubated in 10% serum for 6 h at 37 °C and their migratory positions were monitored using a Cy5.5 filter set.

2.2. Characterizations of CNPs and PTX-CNPs

The average size and morphological shapes of Cy5.5 labeled CNPs and PTX-CNPs in distilled water or PBS were measured using dynamic light scattering (1 mg/ml in PBS) (see Supplementary information, Fig. S1) and transmission electron microscopy (TEM) (1 mg/ml in distilled water). The deformability of CNPs was evaluated using a simple filtration test described as follows. 100 μl of Cy5.5-labeled CNPs solution (1 mg/ml) in PBS was continuously passed through syringe filter membranes (cellulose acetate, Millipore) with decreasing pore sizes (0.8, 0.45, and 0.2 μm). After the filtration test, NIRF images of the filtered solution were observed using a 12-bit CCD camera (Kodak Imaging Station 4000 MM, New Haven, CT) equipped with a Cy5.5 bandpass emission filter set (680 to 720 nm; Omega Optical). The stability of Cy5.5-labeled CNPs was confirmed by measuring the molecular weight changes of each sample following incubation with or without 10 wt.% serum in PBS at 37 °C for 6 h. Both samples of Cy5.5-labeled GC polymer and Cy5.5-labeled CNPs (1 mg/ml) were dissolved in reaction buffer (10 mM Tris–HCl (pH 7.5), 150 mM NaCl, and 1 mM EDTA) with or without 10 wt.% serum at 37 °C. After incubation for 6 h, each sample was loaded onto a vertical slab gel consisting of a 5% stacking gel and a 10% separating gel. All gels were run at a constant voltage (120 V) in a Tris/glycine/SDS buffer. After the SDS-PAGE test, NIRF images of the gels were obtained with a 12-bit CCD camera equipped with a Cy5.5 bandpass emission filter set.

2.3. In vitro drug release profile of the PTX-CNPs

To determine the *in vitro* drug release profile, 10 wt.% PTX-encapsulated CNPs were dispersed in 1 ml of PBS (pH 7.4) by sonication and were placed in cellulose ester membrane tubes (molecular weight cutoff = 12 kDa–14 kDa, Spectrum®, Rancho Dominquez, CA). The test tube was immersed in 10 ml of PBS and gently shaken at 37 °C in a water bath at 100 rpm. Samples of PBS solution were taken at predetermined time intervals and analyzed with isocratic reversed-phase HPLC [14].

2.4. Cytotoxicity of CNPs and PTX-CNPs

Murine squamous cell carcinoma cells (SCC7) were originally obtained from the American Type Culture Collection (Rockville, MD) and cultured in RPMI 1640 (Gibco, Grand Island, NY) containing 10% (v/v) FBS (Gibco) and 1% (w/v) penicillin–streptomycin at 37 °C in a humidified 5% CO_2–95% air atmosphere. Cells were seeded at a density of 5×10^3 cells/well in 96-well flat-bottomed plates, and allowed to adhere overnight. After 2 days post-incubation of each sample in the cell culture system, the cytotoxicity of free PTX dissolved in 50% (v/v) ethanol/Cremophor, CNPs, and PTX-CNPs was measured using MTT assay. The data are expressed as the percentages of viable cells compared to the survival of a control group and were presented as mean ± s.e. ($n=5$).

2.5. Animal models

All animal care and experimental procedures were performed according to the regulation of Kyungpook National University's Animal Care Committee. To generate an early-stage tumor model, athymic C3H-HeJ nude mice (average weight = 20 g) were anesthetized in an isoflurane chamber and 1×10^6 or 3×10^6 SCC7 cells in 50 μl of saline were injected subcutaneously in the pectoral or dorsal sides of mice. After 6, 8, 12, 15, and 18 days, mice were sacrificed and tumor tissues were excised. The time-dependant angiogenic vessel formation of each tumor was confirmed with a rat anti-mouse CD31 monoclonal antibody (Pharmingen, San Diego, CA). After 8 days post-injection, the excised tumor tissues had grown to diameters of between 2.6 ± 0.3 and 6.2 ± 0.5 mm and they showed newly formed angiogenic vessels at their peripheral regions (Supplementary information, Fig. S2). The *in vivo* biodistribution of Cy5.5 labeled CNPs or PTX-CNPs were confirmed by inoculating 3×10^6 SCC7 cells in the dorsal side of male athymic C3H-HeJ nude mice (average weight = 20 g). After the injection of tumor cells, when the tumor reached 7–8 mm in diameter, the mice were used for *in vivo* imaging studies within 10 days.

2.6. In vivo and ex vivo NIRF imaging

In vivo NIRF imaging was performed using a Kodak Image Station 4000 MM. The illumination settings (lamp voltage, filter, and exposure time, etc.) used were identical to those in the animal imaging experiments and all the NIRF emission data were normalized to photons per second per centimeter squared per steradian ($p/s/cm^2/sr$) [12,18]. All fluorescence images were acquired with a ten-second exposure time. The tumors and major organs were dissected and imaged again. For a quantitative comparison, tumor contrasts were calculated by dividing the NIRF intensities at the tumor area by those of normal tissue areas. All data calculated using the regions of interest (ROIs) were drawn over tumor and normal tissues and the results were presented as mean ± s.e. ($n=3$). For histological evaluation, excised tumors and other organs were frozen in Cryomatrix (frozen specimen embedding medium) at −20 °C, and sectioned into 6 μm slices. The NIRF image of each tissue section was viewed by fluorescence microscopy (Carl Zeiss, Oberlcochem, Germany) with a Cy5.5 filter set (Supplementary information, Fig. S4).

2.7. In vivo efficacy studies

The subcutaneous dorsa of C57BL/6 male mice (7 weeks old; 20 g) were inoculated with 3×10^6 SCC7 cells. Mice were divided into four groups ($n=10$), and treated with one of the following treatments: (i) saline, (ii) CNPs, (iii) free PTX (20 mg/kg), and (iv) PTX-CNPs (20 mg/kg). Once the tumor diameter was approximately 7–8 mm, each treatment was administered via a tail vein every three days for 12 days. The tumor volume was recorded for each tumor-bearing mouse for only 18 days since all the free PTX-treated mice were dead within 21 days. The length and width of the tumors were measured by digital calipers, calculating tumor volume using the following formula: $(\text{width}^2\times\text{length})/2$. Also, the survival rate of each group was recorded for 30 days. Eighteen days post-injection, the acute toxicity of each formulation was confirmed by counting the number of WBC after collecting blood samples from normal mice, free PTX-treated mice, and PTX-CNP-treated mice ($n=3$). After 18 days, mice were sacrificed and tumor tissues were isolated. The excised tumors were fixed with 4% (v/v) formaldehyde in PBS (pH 7.4) and sectioned into 6 μm slices. Apoptotic and non-apoptotic cells in tumor tissues were histologically evaluated with hematoxylin and eosin (H&E) staining, DAPI staining and terminal deoxynucleotidyl transferase-mediated nick end labeling (TUNEL) assays, with a commercial apoptosis detection kit (Promega Corp., WI).

2.8. Statistical analysis

Differences between experimental and control groups were determined using one-way ANOVA and deemed statistically significant (indicated by an asterisk (*) in figure) if $p<0.05$.

3. Results

3.1. Physicochemical properties, cellular uptake, and tumor specificity of the CNPs

Glycol chitosan (GC) (Mw = 250 kDa) was modified in the presence of chemical catalysts to introduce 150 ± 4.5 molecules of hydrophobic 5β-cholanic acid per polymer [19,20]. These glycol

chitosan-5β-cholanic acid conjugates were labeled with an average of 4.8 ± 0.7 molecules of monoreactive hydroxysuccinimide Cy5.5, a NIRF imaging agent (Fig. 1B) [10]. When the conjugates were dissolved in aqueous solutions, they spontaneously self-assembled into stable nanoparticles under sonication. Transmission electron microscopy (TEM) and dynamic light scattering analyses of these CNPs revealed that they were spherical with 260 ± 30 nm in diameter (Fig. 1C, Supplementary information, Fig S1). They produced a strong NIRF signal with a Cy5.5 filter set (Fig. 1D), facilitating non-invasive imaging of the nanoparticles in live animals. In phosphate-buffered saline (PBS) at 37 °C, the CNPs remained dispersed and maintained their original average particle size for up to one month (Fig. 1E). Interestingly, although the average size of CNPs was as large as 260 nm, over 95% of the CNPs easily passed through a 0.2-μm filter membrane. This is partly due to the deformable property of CNPs. In contrast, rigid and non-deformable Cy5.5-labeled polystyrene beads (PSs) with 200 nm size were retained on hydrophilic cellulose acetate filters (0.45 μm) (Fig. 1F). In addition, during the SDS-PAGE stability test, CNPs maintained their particulate stability, even after a six-hour incubation in 10 wt.% serum solution (Fig. 1G), which confirmed previous observations that particles composed of numerous polymer conjugates are stable in SDS-PAGE running buffer [21]. In contrast, the linear glycol chitosan (GC) polymers migrated through the gel with ease and are visible in Fig. 1G as the bottom band.

3.2. Tumor targeting efficacy of Cy5.5-labeled CNPs

To evaluate whether the CNPs can indeed specifically target tumors *in vivo*, we used an early-stage tumor model in which murine squamous carcinoma cells (SCC7; 1×10^6 and 3×10^6) were inoculated into the pectoral and dorsal sides of live C3H-HeJ nude mice. After eight days, tumors with different sizes had grown and developed angiogenic vessels around their peripheral regions, a hallmark of early-stage tumors, as confirmed by CD31 immunoassay (Supplementary information, Fig. S2). To visualize different early-stage tumors in mice, 3.3 μmol of Cy5.5-labeled CNPs (5 mg/kg) was administrated intravenously into the tail vein. At one day post-injection, both pectoral and dorsal early-stage tumors were clearly delineated from the surrounding normal tissue, demonstrating the tumor targeting specificity of CNPs, wherein the NIRF signal is proportional to tumor size (2.6 ± 0.3 mm; solid arrows, 6.2 ± 0.5 mm, dot arrows) (Fig. 2A). The excised smaller pectoral tumor (size = 2.6 mm) was positive for tumor cells, according to hematocxylin and eosin (H&E)- and DAPI-stained images, and angiogenic vessels had developed around the tumor's peripheral region, as demonstrated by a CD-31 immunoassay (Fig. 2B). NIRF images revealed that the Cy5.5-labeled CNPs accumulated throughout the tumor tissue. In control experiments, Cy5.5, GC, and CNPs, all with equimolar amounts of Cy5.5 (0.16 μmol), were intravenously injected into the SCC7 tumor-bearing nude mice (Fig. 2C). 1 h after injecting the Cy5.5-labeled GC polymers and CNPs, strong fluorescence was observed throughout the entire animals. Mice treated with free Cy5.5 showed the minimum NIR fluorescence, due to the rapid clearance of the dye from the body. At 12 h post-injection of GC and CNPs, the NIRF images revealed clearly delineated tumors. Importantly, in mice treated with CNPs, tumors showed undiminished fluorescent intensity for up to 3 days, but in mice treated with water-soluble GC, the NIRF signal within the tumors rapidly decreased after 1 day post-injection. The substantially higher tumor contrast (tumor to background (muscle) ratio) in CNP-treated mice as compared with those given water-soluble GC or free Cy5.5 suggested that the CNPs preferentially accumulated in tumor tissues (Fig. 2D).

3.3. Time-dependent biodistribution of CNPs

We subsequently monitored the time-dependent *in vivo* biodistribution of the CNPs after intravenous injection into nude mice bearing pectoral subcutaneous SCC7 tumors of about 7–8 mm in diameter (Fig. 3A). The mice treated with 3.3 μmol of CNP (5 mg/kg) showed a strong NIRF signal throughout the whole body within 1 h of injection, indicating that the CNPs rapidly circulated in the blood-stream. Subcutaneous tumors could be delineated from the surrounding background tissue at 12 h post-injection, and they exhibited a maximum NIR signal beginning at 1 day post-injection. It should be noted that the tumors maintained this maximal NIRF intensity for 3 days, but the NIRF signal persisted for up to 10 days post-injection, with a gradual decrease in signal in the tumor. Fig. 3B shows the higher tumor contrasts as compared with control muscle tissues. The NIRF signal in tumors was 6 times higher than that in muscle at 1 day post-injection, and it gradually decreased over the course of ten days. Upon *ex vivo* evaluation of excised tissues (liver, lung, spleen, kidney, heart, and the tumors themselves), we observed by far the strongest NIRF intensity in the tumor tissue. This indicated that the CNPs were mainly taken up by the tumors, whereas the CNP uptake in normal tissues was not predominant (Fig. 3C). Also, NIRF microscopy of *ex vivo* tumor specimens revealed the strongest NIRF intensity, but negligible NIRF signal was observed in normal tissues (Supplementary information, Fig. S3). In addition, the NIRF total photon counts per gram of each organ from tumor tissues were 4–7 folds higher than those from other organs, providing a decisive evidence that the tumor targeting property of CNPs is much higher than the controls (Fig. 3D).

3.4. In vivo fate of the anticancer drug-loaded CNPs

To utilize the CNPs as a theragnostic agent, CNPs were loaded with an anticancer agent and evaluated whether harboring a therapeutic agent changed their *in vivo* distribution. For these experiments, paclitaxel (PTX, Fig. 4A) was encapsulated into the Cy5.5-labeled CNPs to examine whether the nanoparticles could facilitate drug delivery concurrently with early-stage tumor imaging (Fig. 4A). A dialysis method allowed successful loading of 10% (w/w) PTX into the Cy5.5-labeled CNPs (PTX-CNPs) with as high drug loading efficiency as 92%. The hydrophobic PTX was easily incorporated into the hydrophobic 5β-cholanic acid inner multicores of CNPs [14]. Conceivably, this PTX-CNPs could minimize adverse effects, namely anaphylaxis and severe hypersensitivity, of the current PTX formulation attributed to the Cremophore EL and ethanol used for solubilizing free PTX [22]. The average mean diameter of PTX-CNPs slightly increased from 260 nm to 310 nm with drug loading (Fig. 4B, Supplementary information, Fig. S1), and they were stable under aqueous conditions for up to one month. Fig. 4C shows the release profiles of PTX-CNPs in PBS (pH 7.4, 37 °C). Over the first 6 h, the CNPs quickly released 35% of their PTX, followed by a sustained release of the remaining PTX.

To test and optimize the theragnostic particle-based protocol in our murine tumor model, different formulations of PTX-CNPs (5, 10, or 20 mg PTX/kg) were prepared by correlating the encapsulated PTX concentration to the NIRF intensity of each nanoparticle. Each formulation was intravenously administered to nude mice harboring 7–8 mm SCC7 tumors and the outcome was quantified through NIRF imaging (Fig. 4E). The NIRF intensities within the tumors increased with respect to the drug concentration, demonstrating the dose-dependent delivery of these theragnostic nanoparticles to the tumors. The NIRF intensity in tumor tissues also proportionally increased with the frequency of injections up to a maximum three-day spacing, in that the tumors exhibited strong NIRF signals for up to 3 days post-injection, after which the NIRF signal decreased gradually. The theragnostic efficacy of PTX-CNPs could be maximized by repeating the injections every third day. Of note, the tumor contrast (tumor to muscle ratio) proportionally increased according to the drug concentration and repeated injection time, indicating the excellent tumor targeting specificity of PTX-CNPs in tumor-bearing mice (Fig. 4F). At this optimal protocol, repeated injections of PTX-CNPs at three-day intervals could greatly increase the drug concentration in target tumors, resulting in enhanced therapeutic efficacy of the nanoparticulate CNP formulation with minimized toxicity to normal tissues. *Ex vivo* tissue specimen analysis clearly demonstrated that in the dose-dependent

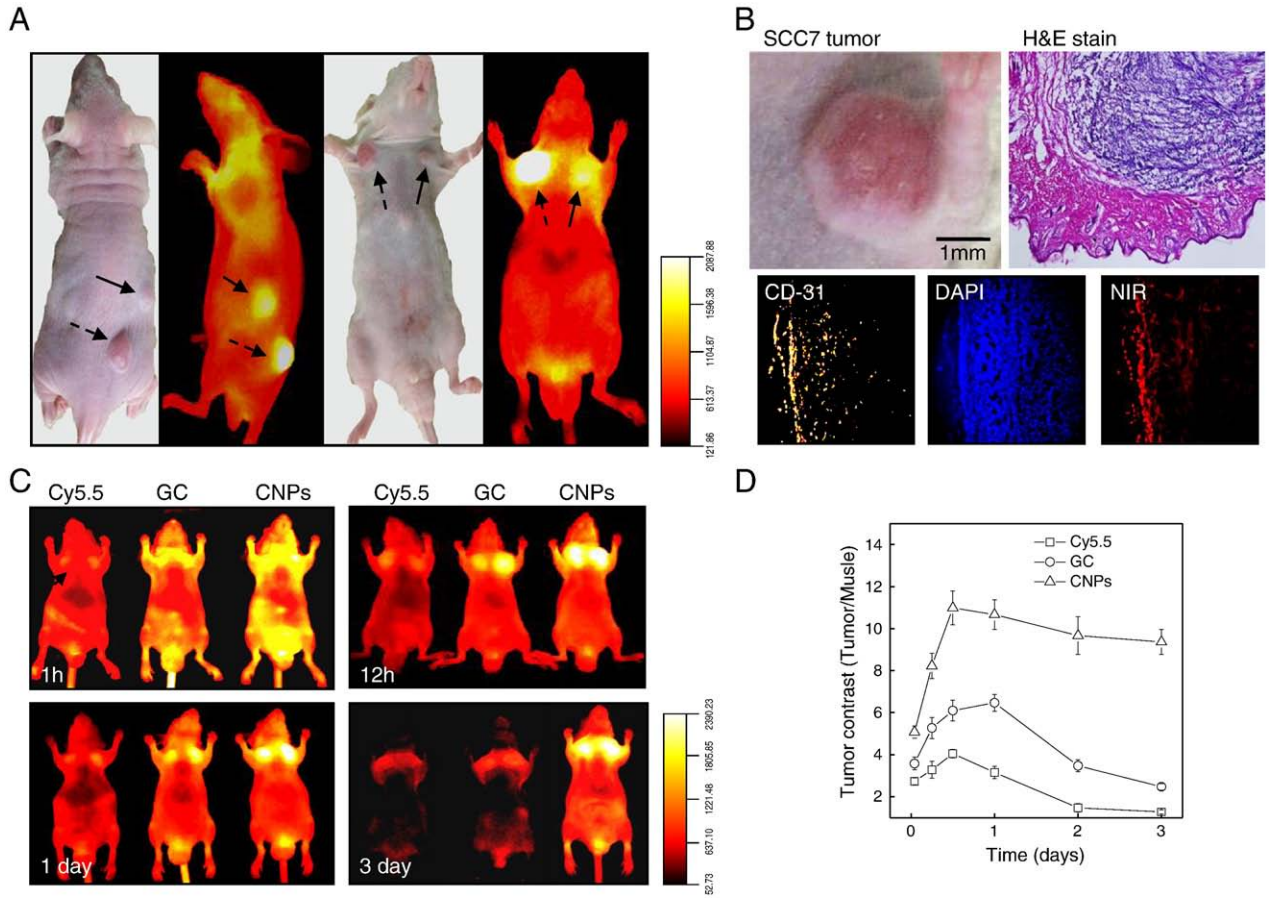

Fig. 2. (A) *In vivo* imaging of Cy5.5-labeled CNPs in tumor-bearing mice. The early-stage tumor models were generated by injecting subcutaneously 1×10^6 or 3×10^6 SCC7 cells into the pectoral and dorsal sides of C3H-HeJ nude mice. After eight days, different size of tumors had grown to 2.6 ± 0.3 mm (solid arrow) and 6.2 ± 0.5 mm (dotted arrow). At 1-day post-injection of 3.3 μmol of Cy5.5-labeled CNPs (5 mg/kg), the NIRF images were obtained using a 12-bit CCD camera equipped with a Cy5.5 bandpass emission filter (NIRF signal scale: 121–2087). (B) The smaller pectoral tumor was positive for tumor cells, as confirmed by H&E staining. Fluorescence microscopic images show the CD-31-positive angiogenic vessels (yellow) and DAPI-stained tumor cells (blue). Intravenously injected, Cy5.5-labeled CNPs were visualized in tumor tissues (red) (original magnification × 100). (C) Time-dependent tumor targeting specificity of free Cy5.5, Cy5.5-labeled GC polymers, and Cy5.5-labeled CNPs, all with equimolar amounts of Cy5.5 (0.16 μmol), in SCC7 tumor-bearing mice (tumor diameter = 7–8 mm). (NIRF signal scale: 52–2390). (D) Tumor to background (muscle) ratio as a function of time after administration of Cy5.5, Cy5.5-labeled GC polymers, and Cy5.5-labeled CNPs in SCC7 tumor-bearing mice. All data represent mean ± s.e.

tumor targeting ability of PTX-CNPs; even when high doses of PTX-CNPs were administered twice over a three-day period, the NIRF intensity from the normal tissue (except the liver) was barely detectable above the background levels (Fig. 4G). With regard to liver tissues, NIRF increased with the drug concentration, but the intensity was consistently much lower than that from the tumors.

3.5. Theragnostic potential of PTX-CNPs

In addition to confirming tumor-specific targeting, NIRF imaging was also utilized to directly monitor tumor growth rate in response to Cy5.5-labeled PTX-CNP administration in live animals. This is to demonstrate that our theragnostic particles could noninvasively track therapeutic efficacy.

Fig. 5A shows the tumor specificity of the PTX-CNPs (20 mg/kg PTX) and the resulting tumor growth rates of the SCC7 tumors (about 7–8 mm in diameter). As before, the NIRF signal from the tumor tissue increased proportionally with the number of Cy5.5-labeled PTX-CNP injections, up to 5 times in 3 days (solid arrows), confirming the tumor targeting specificity of PTX-CNPs. When tumor growth was monitored over a period of 18 days, the NIRF images showed that in control mice, the tumor growth rate rapidly increased (data not shown), but tumors maintained a constant size in mice given five repeated injections of CNPs. After the final injection at day 15, the tumor growth subsided, due to the anticancer effect of PTX within the CNPs. In these optimization studies, the therapeutic nanoparticles successfully mediated both drug delivery and molecular imaging in our nude mouse model.

The optimized treatment protocol, derived from our NIRF imaging data, was used to evaluate the detailed therapeutic efficacy of CNPs in an immunocompetent mouse model, SCC7 tumor-bearing C57BL/6 male mice. After their subcutaneous tumors grew to 7–8 mm in diameter, comparative efficacy studies were performed by dividing the animals into five groups ($n=10$ per group) in a way that minimized tumor size differences among the groups. Using the previously-reported maximal tolerated dose (MTD) of 20 mg/kg for PTX as a reference point [21], we administered the following formulations, using four intravenous injections every third day: (i) saline, (ii) empty CNPs, (iii) PTX (20 mg/kg) in ethanol/Cremophore solution, and (iv) PTX-CNPs (20 mg/kg encapsulated PTX) in saline. Therapeutic efficacy was examined by measuring tumor volumes over the course of 18 days (Fig. 5B). The measurement was limited to 18 days, because all mice treated with free PTX were dead within 21 days. The results demonstrated that administration of free PTX and PTX-CNPs significantly suppressed tumor growth as compared with vector controls (saline and empty CNPs). Treatment with saline or empty CNPs did not mediate any therapeutic efficacy, and the mean tumor volumes at the end of the study for these groups were 8000 mm^3 and 7900 mm^3, respectively. The PTX-CNP-treated mice

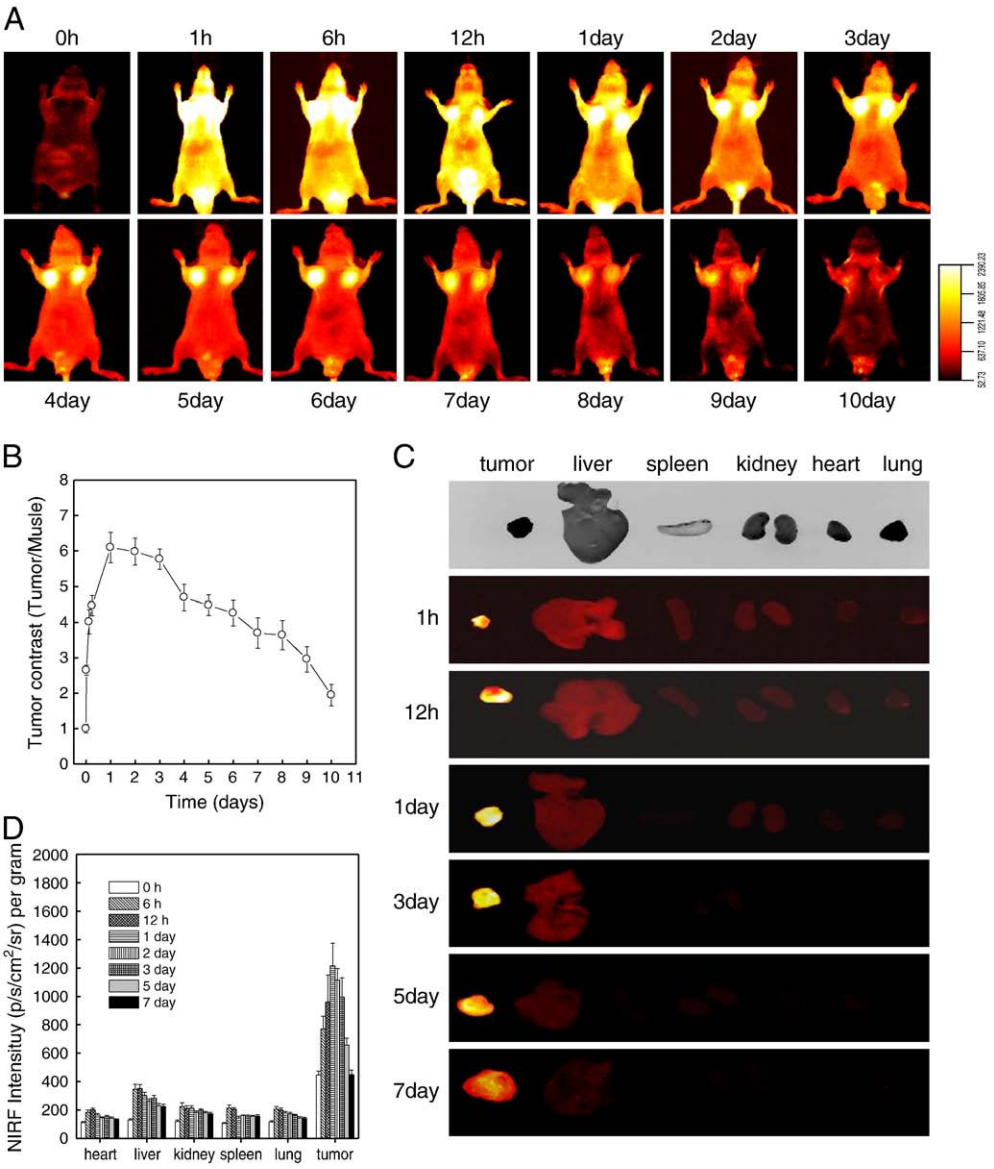

Fig. 3. (A) *In vivo* biodistribution of Cy5.5-labeled CNPs in SCC7 tumor-bearing mice. After tumor diameters reached 7–8 mm, 3.3 μmol of Cy5.5-labeled CNPs (5 mg/kg) were intravenously injected into the tumor-bearing C3H/HeN nude mice. (NIRF signal scale: 45–2680). (B) Time-dependent tumor contrast after administration of Cy5.5-labeled CNPs into tumor-bearing mice ($n=3$). (C) NIRF images of the dissected major organs harvested from Cy5.5-labeled CNP-treated mice. The first row represents the bright field images of individual organs. A strong NIRF signal was observed in tumor tissues at all experimental times. (D) *Ex vivo* imaging of SCC7 xenograft tumor showed higher NIRF signal than other organs at all time points. A quantification of *in vivo* targeting characteristics of Cy5.5-labeled CNPs was recorded as total photons per centimeter squared per steradian (p/s/cm^2/sr) per milligram of each organ at all time points ($n=3$ mice per group). All data represent mean ± s.e.

demonstrated that in the most dramatic reduction in tumor volume; the final mean tumor load was 1000 mm^3 by the end of the study (mean ± s.e., $n=4$, ANOVA at 95% confidence interval), significantly smaller than in mice given the free PTX formulation (2400 mm^3). These results suggested that the superior tumor specificity of PTX-CNPs might have enhanced the efficacy of the anticancer drug, increasing the therapeutic drug concentration in tumor tissues. We also performed histological staining of the excised tumors, and an independent pathologist evaluated the slides. Median tumors excised from PTX-CNP-treated mice exhibited a reduction in the number of cancerous cells and an increase in apoptotic cell nuclei, as demonstrated by H&E staining and TUNEL assays, respectively (Fig. 5C). In contrast, the saline- and empty CNP-treated tumors contained larger numbers of tumor cells and exhibited few signs of apoptosis. Importantly, PTX-CNP treatment greatly enhanced mouse survival rates (Fig. 5D). Eight of the 10 PTX-CNP-treated mice survived the 30-day study, but all the mice in the free PTX-treated groups had succumbed by day 21, most likely due to the severe toxicity of the free PTX formulation. Within the control groups, only 6 and 5 mice from the saline- and empty CNP-treated mice, respectively, survived to the end of the experiment, due to rapid unchecked tumor growth. These results, supported by our *in vitro* cytotoxicity studies, suggested that the PTX-CNPs enhanced the tumor-specific delivery of PTX while curtailing its associated cytotoxicity. In addition, to assess the acute toxicity of each treatment regimen *in vivo*, we analyzed WBC counts within each experimental group after 18 days of treatment (Fig. 5E). The free PTX-treated mice showed substantially reduced WBC counts, compared to PTX-CNP-treated mice. These results indicated that encapsulating the PTX within the nanoscale particles greatly reduced its severe toxicity [14].

4. Discussion

There has been considerable interest in the development of nanotechnology platforms to diagnose and treat cancer by using targeted delivery and controlled drug release. Many approaches have been proposed to develop nanoparticle constructs containing a

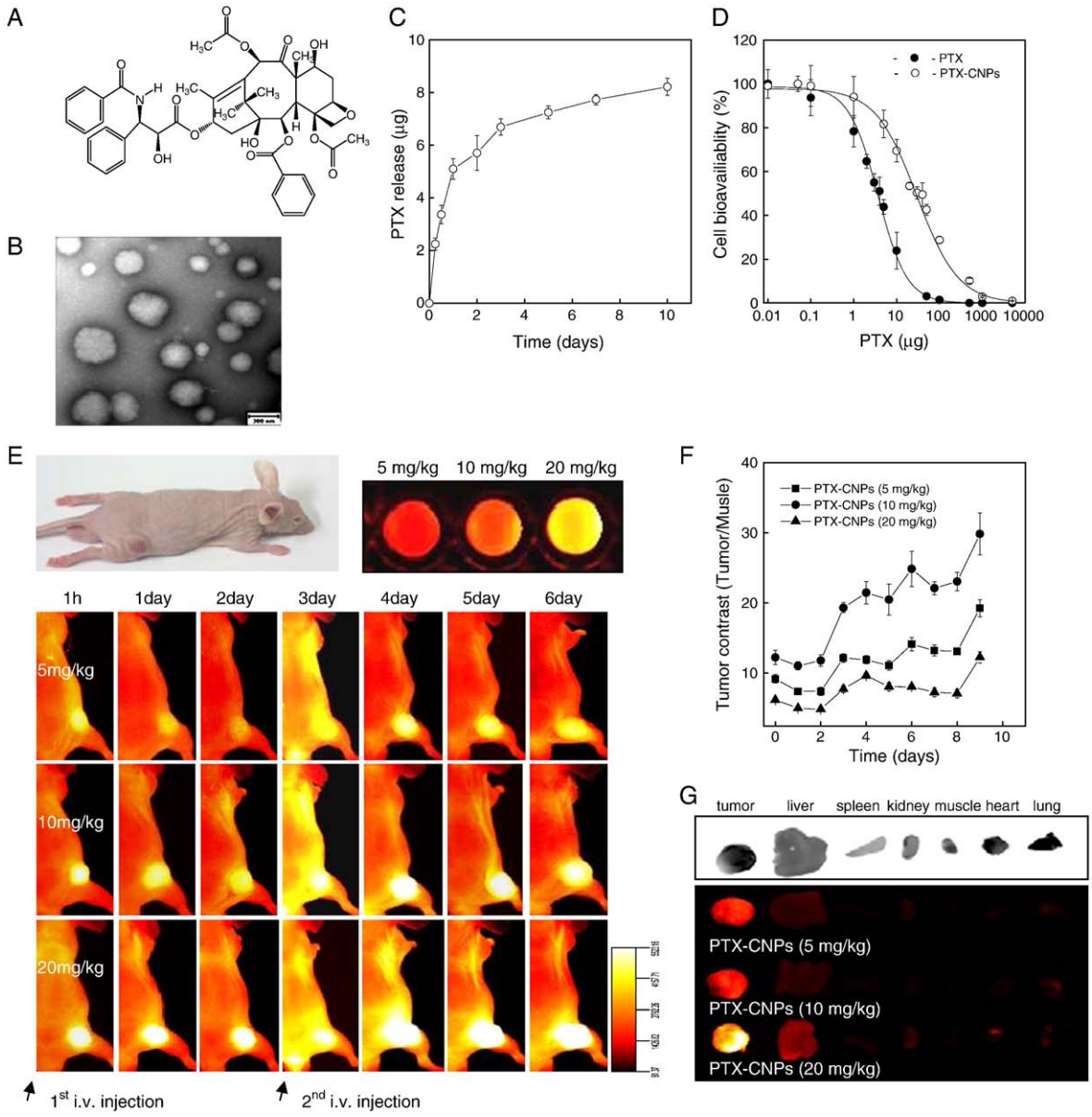

Fig. 4. (A) Chemical structure of paclitaxel (PTX). (B) A TEM image of 1 mg/ml of PTX-CNPs encapsulated with 10% PTX (w/w). (C) A PTX release profile of 10% PTX (w/w)-encapsulated PTX-CNPs in PBS (pH 7.4, 37 °C) ($n=5$). All data represent mean ± s.e. (D) Cytotoxicity of free PTX and PTX-CNPs in cell culture. Predetermined concentrations of PTX and PTX-CNPs were incubated with 5×10^3 SCC7 tumor cells/well in 96-well plates for 48 h. (E) Cy5.5-labeled PTX-CNP doses at different PTX concentrations (5 mg/kg, 10 mg/kg, and 20 mg/kg) were intravenously injected into the SCC7 tumor-bearing mice every third days. The black arrow indicates intravenous injection of Cy5.5-labeled PTX-CNPs. The NIRF signal proportionally increased with dose and injection time (NIRF signal scale: 61–5523). (F) A quantification of the *in vivo* targeting characteristics of Cy5.5-labeled PTX-CNPs was recorded as tumor contrast to background (muscle) as a function of drug concentration and injection frequency ($n=3$). All data represent mean ± s.e. (G) NIRF images of dissected organs harvested from Cy5.5-labeled PTX-CNP-treated mice.

targeting moiety, such as antibody, aptamer, and small molecular ligand, for optimized tumor homing with reduced nonspecific accumulation [22,23]. These targeting moieties showed selective delivery of nanoparticles into tumors or selective detection in tumors. Despite of their improved selectivity, they still have to overcome an obstacle that large percentages of nanoparticles continue to accumulate in the liver and spleen. Conventional wisdom in tumor targeting is based on the EPR effect of nanoparticles, and so it has been assumed that all nanoparticles, as long as the size is in the range of 200 nm or less, will automatically go to the solid tumor by the EPR effect [3–5]. However, the amount of a nanodelivery system delivered to the tumor site is only slightly larger than that of the control. Apparently, nanoparticulate delivery systems are not working well as we all expected. In contrast with the conventional nanocarriers, however, the CNPs used in this study progressively accumulated in the tumor tissues by the EPR effect within 24 h and lasted up to 10 days with considerably low uptake in the liver and spleen.

The efficiency of the EPR effect *in vivo* was significantly affected by different types of carriers regardless of size. In this study, the deformable CNPs showed highest tumor-targeting efficiency. The *in vivo* clearance rate was notably determined by the size and the deformability of the nanoparticles. Generally, nanoparticles of 150–300 nm are mainly found in the liver and the spleen [24]. Therefore, the size of engineered long-circulatory nanoparticles must be either smaller than the critical size or deformable enough in order to avoid the *in vivo* filtration systems. *In vivo*, this deformability might enable these CNPs to pass through biological barriers, such as micro-size blood vessels and membranes in the body. In addition, the rapid cellular uptake characteristic of the CNPs facilitates delivery of anti-cancer drugs and imaging agents into the cytoplasmic compartment

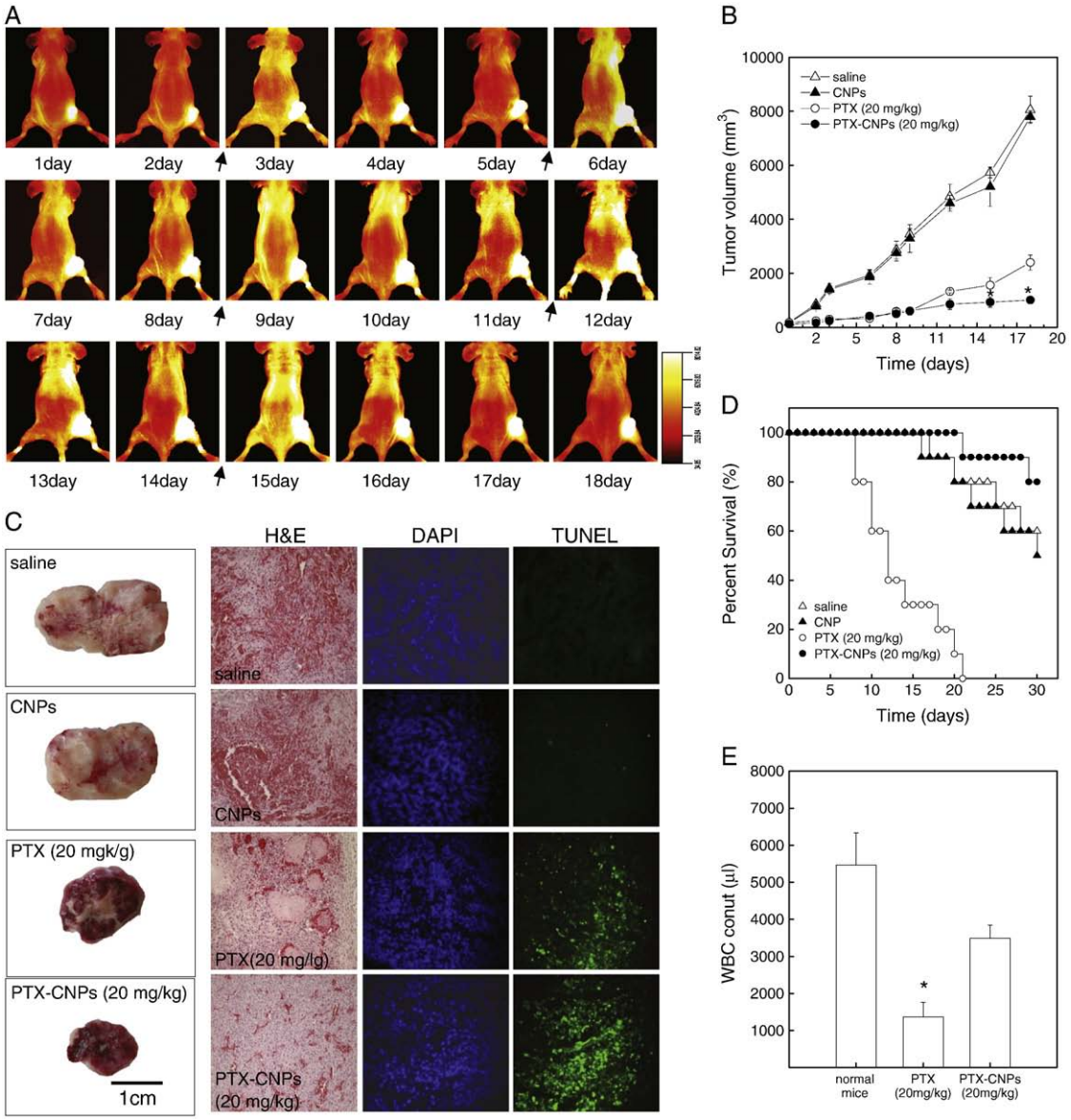

Fig. 5. (A) *In vivo* images of tumor specificity and tumor growth rate in Cy5.5-labeled PTX-CNP (20 mg/kg of free PTX)-treated mice (NIRF signal scale: 34–8014). Cy5.5-labeled PTX-CNPs were injected to tumor-bearing mice four times every three days. The black arrow indicates intravenous injection of Cy5.5-labeled PTX-CNPs. (B) Comparative therapeutic efficacy studies of PTX-CNPs in SCC7 tumor-bearing C57BL/6 male mice ($n = 10$, tumor diameter was 7–8 mm). Tumor size was observed for 18 days. Data represent mean ± s.e. *, data points for the PTX-CNP-treated group that were statistically significant compared to all other groups by ANOVA at 95% confidence interval. (C) Representative images of excised tumors treated with saline, CNPs, free PTX, and PTX-CNPs for 18 days. Histopathological analysis with H&E, DAPI, and TUNEL stainings of each dissected tumor tissue (original magnification × 100). (D) Survival curves demonstrated that 90% of the PTX-CNPs group survived to day 30, whereas the entire PTX-treated group succumbed within 18 days. (E) The acute toxicity of the different formulations was confirmed by WBC counting at seven days post-treatment ($n = 3$ mice per group). All data represent mean ± s.e.

of target tumor cells [15]. The exact mechanism of rapid cellular uptake is not clearly understood yet, but the nanoparticulate structure is critical, as linear water-soluble GC polymer is not taken up by the cells. Taken together, we can suggest that the unique characteristics of the CNPs that we observed *in vitro* (i.e., stability in blood, deformability, and rapid cellular uptake) may have contributed significantly to their tumor targeting by the EPR effect *in vivo*.

5. Conclusion

In conclusion, we developed and characterized the theragnostic CNPs which deliver a fluorescent probe for live imaging and PTX for cancer treatment, simultaneously. These therapeutic CNPs accumulated at the tumor tissues much more efficiently than water-soluble linear polymer or polystyrene beads. The fast cellular uptake of the CNPs resulted in higher therapeutic efficacy. The NIRF label allowed us to noninvasively monitor the *in vivo* fate of the nanoparticles in live animals. Under the optimized treatment protocol, administration of PTX-loaded CNPs greatly diminished tumor size while minimizing the severe toxicity associated with free PTX administration. Furthermore, our results suggested that this methodology could be used to evaluate the performance of other nanoscale drug carriers in cancer therapy, without sacrificing a large number of animals. We anticipate cancer theragnosis with these CNPs presents a new strategy in cancer treatment, in which early-stage cancer diagnosis, drug delivery, and real-time non-invasive monitoring for therapeutic efficacy are carried out simultaneously.

Acknowledgments

This work was financially supported by the Real-Time Molecular Imaging Project, F104AA01003-06A0101-00310, the GRL Program of MEST, by a Korea Research Foundation Grant funded by the Korean

Government (MOEHRD, Basic Research Promotion Fund) (KRF-357-2007-1-D00130), by a grant to the Intramural Research Program of KIST (Theragnosis), by a grant of the Ministry of Health Welfare and Family Affairs (A062254), and by the Advanced Medical Technology Cluster for Diagnosis and Prediction at Kyungpook National University, awarded by MOCIE.

Appendix A. Supplementary data

Supplementary data associated with this article can be found, in the online version, at doi:10.1016/j.jconrel.2010.04.004.

References

[1] V. Ozdemir, B. Williams-Jones, S.J. Glatt, M.T. Tsuang, J.B. Lohr, C. Reist, Shifting emphasis from pharmacogenomics to theragnostics, Nat. Biotechnol. 24 (2006) 942–946.
[2] R. Weissleder, Molecular imaging in cancer, Science 312 (2006) 1168–1171.
[3] W. Arap, R. Pasqualini, E. Ruoslahti, Cancer treatment by targeted drug delivery to tumor vasculature in a mouse model, Science 279 (1998) 377–380.
[4] D. Peer, J.M. Karp, S. Hong, O.C. Farokhzad, R. Margalit, R. Langer, Nanocarriers as an emerging platform for cancer therapy, Nat Nanotechnol 2 (2007) 751–760.
[5] I. Brigger, C. Dubernet, P. Couvreur, Nanoparticles in cancer therapy and diagnosis, Adv Drug Deliv Rev 54 (2002) 631–651.
[6] Y. Matsumura, H. Maeda, A new concept for macromolecular therapeutics in cancer chemotherapy: mechanism of tumoritropic accumulation of proteins and the antitumor agent smancs, Cancer Res. 46 (1986) 6387–6392.
[7] D. Papahadjopoulos, T.M. Allen, A. Gabizon, E. Mayhew, K. Matthay, S.K. Huang, K.D. Lee, M.C. Woodle, D.D. Lasic, C. Redemann, et al., Sterically stabilized liposomes: improvements in pharmacokinetics and antitumor therapeutic efficacy, Proc Natl Acad Sci U S A 88 (1991) 11460–11464.
[8] Y. Matsumura, T. Hamaguchi, T. Ura, K. Muro, Y. Yamada, Y. Shimada, K. Shirao, T. Okusaka, H. Ueno, M. Ikeda, N. Watanabe, Phase I clinical trial and pharmacokinetic evaluation of NK911, a micelle-encapsulated doxorubicin, Br. J. Cancer 91 (2004) 1775–1781.
[9] G.M. Barratt, Therapeutic applications of colloidal drug carriers, Pharm Sci Technolo Today 3 (2000) 163–171.
[10] K. Park, J.H. Kim, Y.S. Nam, S. Lee, H.Y. Nam, K. Kim, J.H. Park, I.S. Kim, K. Choi, S.Y. Kim, I.C. Kwon, Effect of polymer molecular weight on the tumor targeting characteristics of self-assembled glycol chitosan nanoparticles, J Control Release 122 (2007) 305–314.
[11] H.S. Yoo, J.E. Lee, H. Chung, I.C. Kwon, S.Y. Jeong, Self-assembled nanoparticles containing hydrophobically modified glycol chitosan for gene delivery, J Control Release 103 (2005) 235–243.
[12] Y.J. Son, J.S. Jang, Y.W. Cho, H. Chung, R.W. Park, I.C. Kwon, I.S. Kim, J.Y. Park, S.B. Seo, C.R. Park, S.Y. Jeong, Biodistribution and anti-tumor efficacy of doxorubicin loaded glycol-chitosan nanoaggregates by EPR effect, J Control Release 91 (2003) 135–145.
[13] J.H. Park, S. Kwon, J.O. Nam, R.W. Park, H. Chung, S.B. Seo, I.S. Kim, I.C. Kwon, S.Y. Jeong, Self-assembled nanoparticles based on glycol chitosan bearing 5beta-cholanic acid for RGD peptide delivery, J Control Release 95 (2004) 579–588.
[14] S.C. Kim, D.W. Kim, Y.H. Shim, J.S. Bang, H.S. Oh, S. Wan Kim, M.H. Seo, In vivo evaluation of polymeric micellar paclitaxel formulation: toxicity and efficacy, J Control Release 72 (2001) 191–202.
[15] H.Y. Nam, S.M. Kwon, H. Chung, S.Y. Lee, S.H. Kwon, H. Jeon, Y. Kim, J.H. Park, J. Kim, S. Her, Y.K. Oh, I.C. Kwon, K. Kim, S.Y. Jeong, Cellular uptake mechanism and intracellular fate of hydrophobically modified glycol chitosan nanoparticles, J Control Release 135 (2009) 259–267.
[16] K.H. Min, K. Park, Y.S. Kim, S.M. Bae, S. Lee, H.G. Jo, R.W. Park, I.S. Kim, S.Y. Jeong, K. Kim, I.C. Kwon, Hydrophobically modified glycol chitosan nanoparticles-encapsulated camptothecin enhance the drug stability and tumor targeting in cancer therapy, J Control Release 127 (2008) 208–218.
[17] J.H. Kim, Y.S. Kim, S. Kim, J.H. Park, K. Kim, K. Choi, H. Chung, S.Y. Jeong, R.W. Park, I.S. Kim, I.C. Kwon, Hydrophobically modified glycol chitosan nanoparticles as carriers for paclitaxel, J Control Release 111 (2006) 228–234.
[18] J.H. Kim, Y.S. Kim, K. Park, S. Lee, H.Y. Nam, K.H. Min, H.G. Jo, J.H. Park, K. Choi, S.Y. Jeong, R.W. Park, I.S. Kim, K. Kim, I.C. Kwon, Antitumor efficacy of cisplatin-loaded glycol chitosan nanoparticles in tumor-bearing mice, J Control Release 127 (2008) 41–49.
[19] J.H. Park, Y.W. Cho, H. Chung, I.C. Kwon, S.Y. Jeong, Synthesis and characterization of sugar-bearing chitosan derivatives: aqueous solubility and biodegradability, Biomacromolecules 4 (2003) 1087–1091.
[20] J. Hyung Park, S. Kwon, M. Lee, H. Chung, J.H. Kim, Y.S. Kim, R.W. Park, I.S. Kim, S. Bong Seo, I.C. Kwon, S. Young Jeong, Self-assembled nanoparticles based on glycol chitosan bearing hydrophobic moieties as carriers for doxorubicin: in vivo biodistribution and anti-tumor activity, Biomaterials 27 (2006) 119–126.
[21] J.S. Kloover, M.A. den Bakker, H. Gelderblom, J.P. van Meerbeeck, Fatal outcome of a hypersensitivity reaction to paclitaxel: a critical review of premedication regimens, Br. J. Cancer 90 (2004) 304–305.
[22] F. Gu, L. Zhang, B.A. Teply, N. Mann, A. Wang, A.F. Radovic-Moreno, R. Langer, O.C. Farokhzad, Precise engineering of targeted nanoparticles by using self-assembled biointegrated block copolymers, Proc Natl Acad Sci U S A 105 (2008) 2586–2591.
[23] J.H. Lee, Y.M. Huh, Y.W. Jun, J.W. Seo, J.T. Jang, H.T. Song, S. Kim, E.J. Cho, H.G. Yoon, J.S. Suh, J. Cheon, Artificially engineered magnetic nanoparticles for ultra-sensitive molecular imaging, Nat. Med. 13 (2007) 95–99.
[24] S.M. Moghimi, A.C. Hunter, J.C. Murray, Long-circulating and target-specific nanoparticles: theory to practice, Pharmacol. Rev. 53 (2001) 283–318.